JOURNAL OF MATERIALS SCIENCE 33 (1998) 1571–1578

Kinetics of the anatase–rutile transformation in TiO_2 in the presence of Fe_2O_3

F. C. GENNARI*, D. M. PASQUEVICH
Comisión Nacional de Energía Atómica, Centro Atómico Bariloche, (8400) s.c. de Bariloche, Río Negro, Argentina. Consejo Nacional de Investigaciones Científicas y Técnicas
E-mail: gennari@cab.cnea.edu.ar

The anatase–rutile phase transition in TiO_2 in the presence of Fe_2O_3 was investigated in air and argon atmospheres by means of X-ray diffraction and scanning electron microscopy. Isothermal curves of rutile transformed from anatase as a function of time were obtained between 825 and 950 °C. The data were well fitted by various rate laws. In the presence of Fe^{3+}, the anatase–rutile transition temperature is lower and the transformation rate in air is higher than the corresponding one in pure TiO_2. The transformation in the presence of Fe^{3+} in an argon atmosphere is more rapid than in air. The enhancement effect of Fe^{3+} on the anatase–rutile transformation in both atmospheres is understood on the basis of the formation of oxygen vacancies. © *1998 Chapman & Hall*

1. Introduction

It is well known that an isolated crystalline phase is thermodynamically stable only when its free energy is a minimum at a given temperature and pressure [1–3]. On the other hand, when the free energy is a local minimum the phase is thermodynamically metastable. A metastable phase, separated by energy barriers from the stable state, will move to the free energy minimum when it overcomes the kinetic restrictions. Such a behaviour is often observed in metallic oxides having various polymorphs. Titanium dioxide is an example. It has three polymorphs: rutile (tetragonal, $P4_2/mnm$), anatase (tetragonal, $I4/amd$) and brookite (orthorhombic, $Pcab$). Rutile is the only stable phase, whereas anatase and brookite are metastable and irreversibly transform to rutile on heating [4]. The anatase–rutile transformation does not have a transition temperature because there is no phase equilibria involved. For this reason, the anatase–rutile transition does not take place at a defined temperature and was observed at temperatures between 400 and 1000 °C [4], depending upon the characteristics of the anatase powders, such as impurity content [5–8], deviations of stoichiometry, surface area [8], particle size [8], and so forth.

In particular, the anatase–rutile transformation is strongly dependent on the impurity content in TiO_2 [5–13] and the reaction atmosphere [5, 14–16]. Impurities having the most pronounced inhibiting action are chloride, sulphate and fluoride ions [7, 8], whereas impurities that accelerate the transformation include alkaline [5, 6, 13] and transition metal ions [5, 6, 9–13]. It has been proposed [5] that ions increasing the oxygen vacancy concentration in the TiO_2 lattice will accelerate the transformation, whereas ions with a valence higher than 4, which correspondingly reduce the oxygen vacancy concentration, will retard it [5]. For example, the addition of WO_3 [9] inhibits the transformation and the addition of Li_2O [10], K_2O [10], Na_2O [10], Fe_2O_3 [6, 9, 12, 13], CuO [5, 6, 13] and MnO_2 [6, 9, 13] enhances it.

The effect of different reaction atmospheres on the anatase–rutile transformation has been reported [5, 14–16]. It has been shown that vacuum [5, 14, 15], hydrogen [5, 14, 15], static air [15, 16], flowing air [15], oxygen [15], argon [15], nitrogen [15] and chlorine [16] affect the transformation rate to different degrees. Iida and Ozaki [9] have reported that the transformation rate was greater in a hydrogen atmosphere than in a vacuum, whereas an increase in the oxygen partial pressure decreased the rate of transformation. Shannon and Pask [5, 14] have also demonstrated that the transformation was accelerated in a hydrogen atmosphere, whereas in vacuum the transformation was slower than in air [5, 14]. The authors have proposed that the formation of oxygen vacancies, which favour the transition, is predominant in hydrogen, whereas Ti^{3+} interstitial, which inhibits the transformation [5, 14], would be formed in a vacuum. Various authors have proposed that chemically reducing atmospheres enhance the transition because the formation of oxygen vacancies in the anatase lattice favours bond rupture and the diffusion necessary for the crystallographic rearrangement [5, 13, 14]. These lattice defects act as colour centres, changing the

*Author to whom all correspondence should be addressed.

colour of TiO_2 from white to light yellow, grey or dark blue, with increasing non-stoichiometry [17, 18]. Andrade Gamboa and Pasquevich [16] reported the strong accelerating effect of gaseous chlorine on anatase–rutile transformation, and they explained the phenomenon based on oxygen vacancies formation and vapour mass transported by $TiCl_4$(g) contribution.

The kinetics of the anatase–rutile transformation in doped TiO_2 has not been studied extensively [5, 13]. Yoganarasimhan and Rao [8] have reported that the activation energy, E_a, of the transformation of anatase prepared from sulphate hydrolysis was 120 ± 10 kcal mol^{-1} (502 kJ mol^{-1}) compared with 90 ± 10 kcal mol^{-1} (377 kJ mol^{-1}) for pure anatase. Suzuki and Tukuda [11] have studied the transformation in anatase prepared from sulphate and chloride processes. The activation energies were similar within error limits: 105–107 kcal mol^{-1} (439–448 kJ mol^{-1}). Shannon and Pask [5], in the study of the beneficial effect of CuO, found that although the activation energy was increased by 50–70 kcal mol^{-1} (209–293 kJ mol^{-1}), the addition of 1% CuO reduced the transformation temperature by 200 °C. Heald and Weiss [12] have reported that the transition in the presence of 0.1% Fe_2O_3 in hydrogen took place with an activation energy of 124 kcal mol^{-1} (519 kJ mol^{-1}) as compared with 100 kcal mol^{-1} (418 kJ mol^{-1}) for undoped material. MacKenzie [13] has found that the addition of 1 wt % CuO, MnO_2 or Fe_2O_3 reduces the transformation temperature and increases the activation energy by 40–60 kcal mol^{-1} (167–251 kJ mol^{-1}) in comparison with that measured in undoped TiO_2.

In the present work, the kinetics of the anatase–rutile transformation in air in the presence of Fe_2O_3 was studied. Various rate laws were tested and values of activation energy were compared with values given in the literature. In addition, the anatase–rutile transition in the presence of Fe_2O_3 in an argon atmosphere was also investigated.

2. Experimental procedure

2.1. Materials

Samples were prepared by mixing anatase TiO_2, which initially contained 95% anatase–5% rutile (Mallinckrodt Chemical Works) and α-Fe_2O_3 (Spex Industries, Inc., USA) powders in a 7/3 weight ratio. Argon (99.99% purity, AGA, Argentina) was used.

2.2. Procedure

In order to analyse the effect of Fe^{3+} on the anatase–rutile phase transition, samples were placed within a quartz crucible and heated in air, kept at the desired temperature for a selected time and then quenched in air. To study the transformation in the presence of Fe^{3+} in an argon atmosphere, every sample was placed within a quartz tube which was held in vacuum (1.3×10^{-5} MPa) for 1 h and then filled with argon and sealed. The argon pressure was 0.1 MPa at every reaction temperature. The encapsulated samples were introduced in a preheated vertical electric furnace at the reaction temperature for a selected time. After heating, the encapsulated samples were air cooled and broken out of the quartz tubes at room temperature.

After each thermal treatment, the percentages of anatase and rutile were calculated from X-ray powder diffraction (XRD) measurements (PW 1710, Philips Electronic Instruments, Inc.) using nickel-filtered CuK_α radiation. The fraction of rutile in each sample was determined from the relative X-ray diffraction intensity corresponding to anatase [1 0 1], $d = 0.3520$ nm and rutile [1 1 0], $d = 0.3247$ nm, reflections. Then, the mass fraction of rutile, X_R, was determined as follows [19]

$$X_R = 1 \Big/ \left[1 + 1.26 \left(\frac{I_A}{I_R} \right) \right] \quad (1)$$

where I_A and I_R are the mentioned lines of rutile and anatase, respectively.

The samples were also observed with scanning electron microscopy (SEM 515, Philips Electronic Instruments) to characterize the microstructural changes associated with each thermal treatment and atmosphere.

3. Results

3.1. Transformation in air

Fig. 1 shows the XRD patterns corresponding to Fe_2O_3–TiO_2 starting mixture (Fig. 1a) and two examples of samples after thermal treatments in air (Fig. 1b and c). In Fig. 1a, the lines observed at $2\theta = 25.30°$ ($d = 0.3520$ nm) and 48.09° ($d = 0.1892$ nm) correspond to the most intense diffractions of anatase (A), while the weak line at $2\theta = 27.47°$ ($d = 0.3247$ nm) corresponds to the most intense diffraction of rutile (R). Using Equation 1, the TiO_2 intensities ratio reproduces the 5% rutile of the starting TiO_2. The lines at $2\theta = 33.18°$, 35.64° and 54.14°, correspond to the

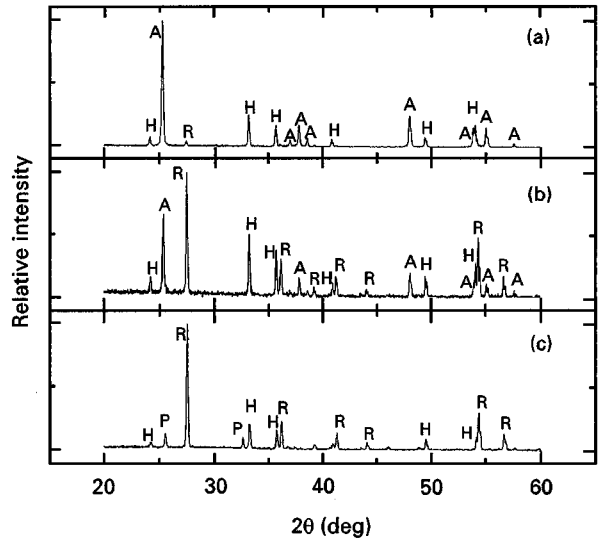

Figure 1 Diffraction patterns of Fe_2O_3–TiO_2 mixtures subjected to different thermal treatment: (a) starting sample, 5% rutile; (b) sample heated in air for 10 h at 870 °C, 72% rutile; (c) sample heated in air for 36 h at 870 °C, 100% rutile. A, anatase; R, rutile; H, haematite; P, pseudobrookite.

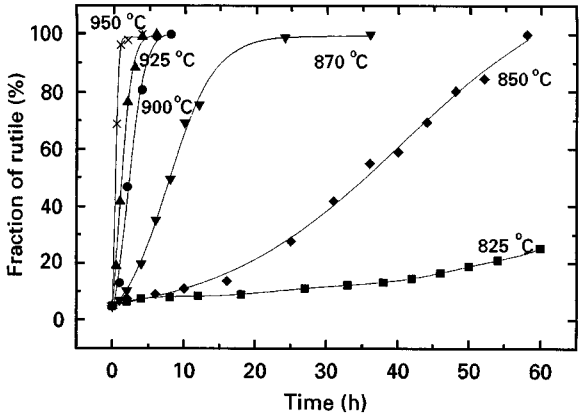

Figure 2 Transformed fraction of rutile (%) in air in the presence of Fe_2O_3 as a function of time at various temperatures.

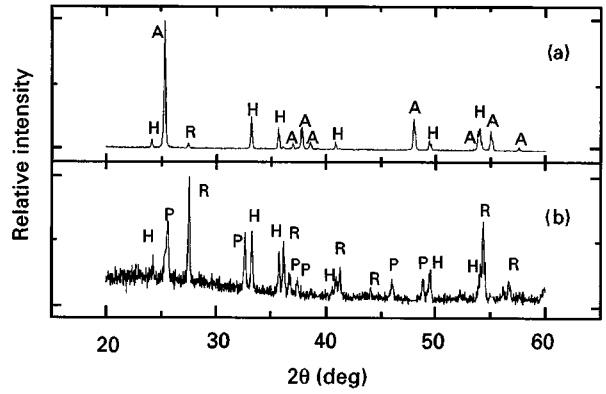

Figure 3 Diffraction patterns of Fe_2O_3–TiO_2 mixtures: (a) starting powder, 5% rutile; (b) powder heated in argon for 0.5 h at 870 °C, 100% rutile.

three most intense lines of the haematite phase of Fe_2O_3(H). Thus, the diffraction pattern of the starting sample shows that the most intense lines of anatase, rutile and haematite do not overlap, so that the three phases can be well analysed by XRD.

When Fe_2O_3–TiO_2 samples were heated in air, the original diffraction pattern of anatase gradually diminished in intensity and was progressively and steadily displaced by the characteristic rutile diffraction pattern, as shown in Fig. 1b. This figure shows a typical diffraction pattern of a Fe_2O_3–TiO_2 sample heated in air for 10 h at 870 °C, containing 72% rutile. When the heating time was increased (36 h), the phase transition was complete. However, new diffraction lines were also observed, as shown in Fig. 1c. These new diffraction lines were observed at $2\theta = 25.58°$ and 32.59° and were indexed as pseudobrookite, Fe_2TiO_5 (P). The formation of pseudobrookite was mainly observed above 870 °C and for long heating times.

Fig. 2 shows, for each temperature, the results of the effect of thermal treatments in air on anatase–rutile transformation as fraction of rutile in TiO_2 as a function of time. The anatase–rutile transformation curves have a typical sigmoidal shape in which the fraction of transformed rutile first increases slowly with time, then much more rapidly, and finally slowly again. Fig. 2 also shows that the transformation was strongly dependent upon the temperature. At 950 °C the transformation was complete in about 4 h, whereas 20% rutile was measured after heating for 60 h at 825 °C.

The microstructure of the TiO_2 powders heated in air was also analysed. The starting powder of TiO_2 was composed of small grains with a mean size of about 0.2 μm, as shown elsewhere [16]. After heating for 10 h in air at 870 °C the grains of TiO_2 powders grow to a grain size of about 0.3–0.35 μm and some grains of 1–1.5 μm indicating a non-uniform distribution of sizes.

3.2. Effect of reaction atmosphere

Fig. 3 shows a comparison of the XRD patterns of Fe_2O_3–TiO_2 starting mixture (Fig. 3a) and the same mixture heated in an argon atmosphere for 0.5 h at 870 °C (Fig. 3b). The X-ray pattern of Fig. 3b is characterized by strong and sharp diffractions lines of rutile, together with sharp lines of pseudobrookite and haematite. The anatase phase (Fig. 3a) transformed completely to rutile in the argon atmosphere in 0.5 h (Fig. 3b), indicating that the transformation was more rapid than in air at the same temperature (see Fig. 2).

TABLE I Fraction of rutile transformed on heating Fe_2O_3–TiO_2 mixtures in argon and in air for several hours at various temperatures

Temperature (°C)	Argon		Air
	Time (h)	Rutile (%)	Rutile (%)
870	0.5	100	20%
	1	100	(4 h)
	4	100	100% (36 h)
825	1	14	
	1,5	24	5%
	2	52	(10 h)
	3	100	
775	1	⩽5	
	4	15	5%
	8	17	(20 h)
	12	20	
	16	28	
	20	67	

Table I summarizes the effect of argon and air atmospheres on the phase transition in the presence of Fe_2O_3 at various temperatures. The transformation was complete in air after 36 h at 870 °C. When the temperature decreased, the transformation was slower, so that it was negligible after heating for 20 h at 775 °C. On the other hand, at the same temperature the anatase transformed in argon to 67% rutile.

The morphology of pseudobrookite formed in both air and argon atmospheres was similar. Fig. 4 shows the morphology of pseudobrookite obtained in an argon atmosphere. A shell of pseudobrookite was found around a haematite particle, as verified by EDXS analysis which indicated a molar ratio Fe/Ti: 2/1 on the shell and Fe 100% in the particle inside the shell.

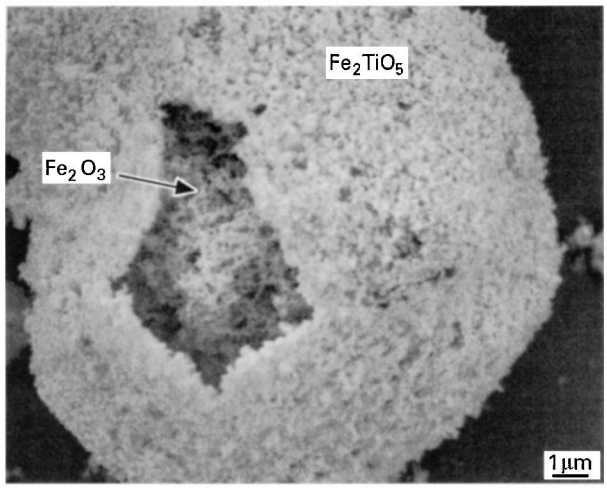

Figure 4 Microstructure of Fe_2TiO_5 formed in an argon atmosphere after heating Fe_2O_3–TiO_2 samples for 0.5 h at 870 °C.

TABLE II Transformed fraction of rutile (%) from pure anatase (in air) as a function of time at various temperatures [20]

Temperature (°C)	Time (h)	Rutile (%)
921	14	9
	36	13
	75	20
950	14	13
	36	24
	56	50
962	14	18
	36	40
	56	72
976	14	26
	36	63
	56	83

4. Discussion

4.1. The enhancement effect of Fe_2O_3 on the phase transition in air

The anatase–rutile transformation in the presence of Fe_2O_3 was well monitored and quantified by XRD analysis, as illustrated in Fig. 1. The three phases, anatase, rutile and haematite, were clearly identified because their most intense diffractions do not overlap. Sharp diffraction lines also indicate that the phases were well crystalline, forming large-grain aggregates. Also, the pseudobrookite phase, Fe_2TiO_5, which was formed at long heating times (Fig. 1c), was also clearly identified by XRD. As it will be discussed later, however, the pseudobrookite was formed on Fe_2O_3 particles by diffusion of TiO_2 into Fe_2O_3 lattice, indicating that its formation is independent of the anatase–rutile transition, which occurred in the TiO_2 lattice.

To analyse the effect of Fe^{3+} on the anatase–rutile transformation, the transformation rate of pure anatase must be known. Assuming that the transformation kinetics may depend upon the microstructure, the comparison must be performed on the same anatase powder. Fortunately, various authors [16, 20] have characterized the transformation in air using the same anatase powder batch used in this study. Table II summarizes such results in pure anatase at various temperatures [20]. The transformation was not observable in the first 10 h at 921 °C, and more than 75 h were needed to achieve 20% rutile. Although the transformation was more rapid when the temperature was increased, the amount of transformed rutile was 50%, 72% and 83% for 50 h at 950, 962 and 976 °C, respectively.

A comparison of Table II with data shown in Fig. 2 reveals that the presence of Fe_2O_3 significantly accelerates the transformation. For example, a full transformation in the presence of Fe_2O_3 was achieved after heating for 4 h at 950 °C, while only 50% rutile transformed in pure anatase after heating for 56 h at 950 °C (Table II). The enhancement effect of Fe_2O_3 on the transformation was also observed at 925 °C, the temperature at which 100% rutile was achieved in 6 h. The presence of Fe_2O_3 also decreased the transition temperature, because the transformation was observable at temperatures as low as 825 °C. Thus, the transition became measurable at about 100 °C lower than in pure TiO_2 [16]. This result is consistent with the temperature decrease observed for the transformation in doped TiO_2 [5–13].

It is well known [5, 13] that the presence of impurities in the TiO_2 lattice affects both the temperature and the activation energy, E_a, of the transformation. Hence, E_a values of the transformation in the absence and presence of Fe^{3+} can be calculated and compared using data presented in Table II and Fig. 2. However, the comparison must be undertaken judiciously because the value of the activation energy may be dependent upon the rate law fitting the data. In fact, Shannon and Pask [5] have demonstrated that the transformation could equally well be expressed by a first order, contracting interface area, and nucleation growth equations, obtaining E_a values of 148, 186 and 194 kcal mol^{-1} (619, 778 and 811 kJ mol^{-1}), respectively. Moreover, Czanderna *et al.* [17] have described the transformation using a second-order rate law and reported $E_a = 110$ kcal mol^{-1} (460 kJ mol^{-1}), while Rao [21] has applied an exponential transformation rate and calculated $E_a = 100$ kcal mol^{-1} (418 kJ mol^{-1}).

According to that, a simple and general method to calculate E_a will be applied, which has the advantage of avoiding the proposal of a rate law for pure TiO_2. This method is based upon the fact that the reaction rate law of many soild-state reactions are of the following form

$$d\alpha/dt = F(\alpha)K(T) \quad (2)$$

where the function $F(\alpha)$ depends on the mechanism controlling the solid-state transformation, and the function $K(T)$ depends upon the absolute temperature, T. The temperature dependence of $K(T)$ can be expressed by an Arrhenius equation $K(T) = A\exp(-E_a/RT)$, where E_a is the activation energy and R is the gas constant. From Equation 2 the activation energy can be determined, even though the $F(\alpha)$ function is unknown. In fact, by rearranging, integrating and taking logarithm of the resulting

TABLE III Several rate laws used to test the anatase–rutile transformation in the presence of Fe_2O_3 in air and correlation coefficients at various temperatures, region of fitting and E_a values obtained for each model

Kinetic law $f(\alpha)$	Model	α range of fitting	Activation energy (kcal mol^{-1})
$\mathrm{Ln}\,\alpha = kt + c$	First order $R = 0.989$ (925 °C) $R = 0.999$ (870 °C) $R = 0.985$ (825 °C)	0.1–0.3	126 ± 7 (527 kJ mol^{-1})
$(1-\alpha)^{1/3} = kt + c$	Contracting spherical interface $R = 0.999$ (925 °C) $R = 0.999$ (870 °C) $R = 0.988$ (825 °C)	0.35–0.85	101 ± 9 (423 kJ mol^{-1})
$\mathrm{Ln}(1-\alpha) = kt + c$	Random nucleation + rapid growth $R = 0.984$ (925 °C) $R = 0.999$ (870 °C) $R = 0.981$ (825 °C)	0.35–0.85	102 ± 12 (427 kJ mol^{-1})
$[\mathrm{Ln}(1-\alpha)]^{1/3} = kt + c$	Nucleation + growth of overlapping nuclei $R = 0.992$ (925 °C) $R = 0.999$ (870 °C) $R = 0.992$ (825 °C)	0.35–0.85	101 ± 15 (423 kJ mol^{-1})

expression, the following equation is obtained

$$\ln t_\alpha = -E_a/RT + \ln\left[A^{-1}\int_0^\alpha d\alpha/F(\alpha)\right] \quad (3)$$

where t_α is the time to achieve a transformation degree α. From the foregoing expression it is possible for a given α to plot $\ln t_\alpha$ versus $1/T$ and the slope of the resulting straight lines gives the value of E_a.

By this method and from data presented in Table II it was determined that at $\alpha = 0.3$, $E_a = 100$ kcal mol^{-1} (418 kJ mol^{-1}), which is of the order of the values reported for pure anatase ($E_a = 110$ kcal mol^{-1} [17] and $E_a = 100$ kcal mol^{-1} [21]). When the transition took place in the presence of Fe_2O_3 (Fig. 2), $E_a =$ 135 kcal mol^{-1} (565 kJ mol^{-1}) at $\alpha = 0.3$ and $E_a = 105$ kcal mol^{-1} (439 kJ mol^{-1}) at $\alpha = 0.8$, were obtained. Thus, the presence of Fe_2O_3 increased the nucleation activation energy in 35 kcal mol^{-1} (146 kJ mol^{-1}) with respect to pure anatase, which agrees with the fact that the activation energy of the transformation in doped anatase using different accelerating impurities was higher than for undoped anatase [5, 13].

4.2. Kinetic analysis of the transition phase in the presence of Fe_2O_3

It is well known [2, 8, 17] that the irreversible anatase–rutile transformation in TiO_2 occurs by a nucleation–growth process. Therefore, some authors [5, 13] have treated the transformation kinetics using rate laws taking into account that the overall rate is diffusion controlled. Hence, the kinetics of the transformation enhanced by impurities has been described using rate laws such as first-order, contracting spherical interface, and nucleation and crystal growth [5, 12, 13]. The first-order kinetics is described by the following equation

$$f_1(\alpha) = \ln\alpha = k_1 t + c \quad (4)$$

where α is the transformed fraction of rutile, k_1 is the rate constant and c is a constant. This relation is based on the assumption of a one-dimensional nucleus and a constant growth rate and it is applied to the nucleation step. For the growth period, the following rate laws have been applied

$$f_2(\alpha) = (1-\alpha)^{1/3} = k_2 t + c \quad (5)$$

$$f_3(\alpha) = \ln(1-\alpha) = k_3 t + c \quad (6)$$

$$f_4(\alpha) = [\ln(1-\alpha)]^{1/3} = k_4 t + c \quad (7)$$

which correspond to a contracting spherical interface (Equation 5), random nucleation and rapid growth (Equation 6) and nucleation and growth of overlapping nuclei (Equation 7).

The data presented in Fig. 2 are useful to test whether the transformation kinetics in the presence of Fe_2O_3 is well described by the foregoing equations. Thus, Equations 4–7 were analysed, representing values of $f(\alpha)$ against time at various temperatures. A linear regression analysis was performed for every function $f(\alpha)$. Table III shows values of the correlation coefficients and activation energies for every $f(\alpha)$. In all cases, a moderate correlation was obtained at each temperature. However, it is noticed that correlations are very similar for all models. Also, the values of E_a (last column in Table III) determined by plotting $\ln k$ against $1/T$ (see Fig. 5) are very close to each other. Considering that the geometry of the rutile crystals is uncertain and the particle size is not uniform, the scattering in the plotted points determined by the different expressions can be considered acceptable. Thus, the four rate laws tested are statistically equally satisfactory to describe the transformation kinetics. The values of E_a obtained are also acceptable, being in agreement with values previously reported for the transformation in the presence of impurities [5, 13]. The only difference between the models tested was the value of $E_a = 126$ kcal mol^{-1} (527 kJ mol^{-1}) corresponding to low values of α. This might indicate

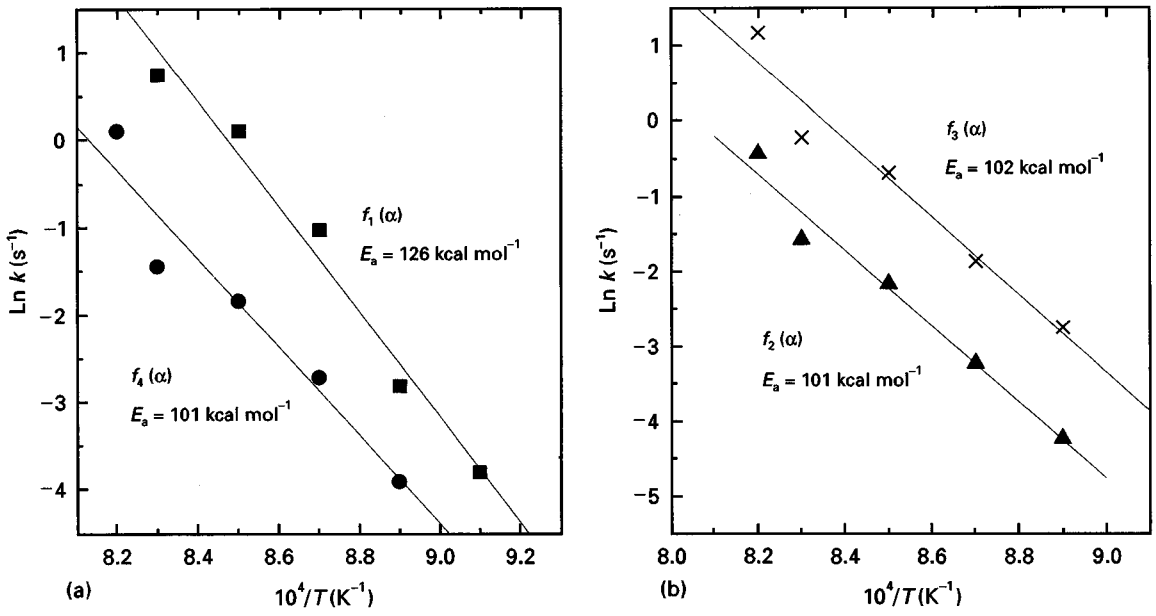

Figure 5 Plots of $\ln k$ versus $1/T$ for models presented in Table III and E_a values calculated from the corresponding slopes. (a) Models $f_1(\alpha)$ and $f_4(\alpha)$. (b) Models $f_2(\alpha)$ and $f_3(\alpha)$.

that the activation energy for the nucleation is greater than that for growth.

As indicated above, models (Equations 4–7) have been used in the literature to describe the anatase–rutile transformation, though they have been earlier developed to describe solid-state reactions such as thermal decomposition and solid–solid chemical reactions [1, 2]. Actually, the first theoretical model to understand nucleation–growth transformations has been formulated by Johnson and Mehl [22] and Avrami [23–25] (JMA model). This theory assumes that the nucleation frequency is either constant or a maximum at the beginning of the transformation and decreases during transformation, so that a nucleation–growth transformation is governed by the following equation [1, 2, 23–25]

$$\alpha = 1 - \exp(-kt^n) \tag{8}$$

where α is the fraction transformed, t is the transformation time and k and n are parameters depending upon the transformation mechanism. When n is greater than unity, the predicted curves are sigmoidal, as widely reported [1–3]. Indeed, curves plotted in Fig. 2 are sigmoidal. Hence, Equation 8 can be employed to analyse the experimental data plotted in Fig. 2. Table IV gives n and k values resulting from testing Equation 8 at various temperatures. The n values, which reflect the growth morphology, range from 1.5–2.4. Such a variation is consistent with a diffusion-controlled transformation characterized by a decreasing nucleation rate, as reported by Christian [1]. The effect of the temperature on k is also in agreement with the theoretical basis of the JMA model, because k depends on the nucleation and growth rates. From values of k the apparent activation energy of the transformation can be obtained. In effect, differentiation of Equation 8 allows the following equation to be written

$$\frac{\partial\alpha}{\partial t} = nk(1-\alpha)t^{n-1} \tag{9}$$

TABLE IV Values of n and k parameters for the JMA equation at different temperatures

Temperature (°C)	n	k
950	1.5 ± 0.3	3.3 ± 0.7
925	1.4 ± 0.1	0.54 ± 0.03
900	1.7 ± 0.2	0.17 ± 0.03
870	1.7 ± 0.1	0.02 ± 0.006
850	2.4 ± 0.2	$(1.6 \pm 0.8) \times 10^{-4}$

which can be rewritten as

$$\frac{\partial\alpha}{\partial t} = nk^{1/n}(1-\alpha)[\ln(1-\alpha)^{-1}]^{(n-1)/n} \tag{10}$$

where $nk^{1/n}$ is a term depending upon the temperature analogue to a chemical rate constant. Assuming that it follows an Arrhenius equation, $E_a = 100\ \text{kcal mol}^{-1}$ ($460\ \text{kJ mol}^{-1}$) is obtained. Analysing in more detail Equation 10, it is noticed that it has the same form as Equation 2. In fact, $nk^{1/n}$ represents the function $K(T)$ of Equation 2, which is a function of temperature, and the remaining factor of Equation 10 represents the function $F(\alpha)$, which reflects the transformation mechanism. Therefore, a determination of E_a as a function of α from Equation 10 should give $E_a = 135\ \text{kcal mol}^{-1}$ ($565\ \text{kJ mol}^{-1}$) at $\alpha = 0.3$ and $E_a = 105\ \text{kcal mol}^{-1}$ ($439\ \text{kJ mol}^{-1}$) at $\alpha = 0.8$, as determined from Equation 3. As a consequence, the value of $E_a = 110\ \text{kcal mol}^{-1}$ ($460\ \text{kJ mol}^{-1}$) obtained from Equation 6 is an average between that of nucleation ($135\ \text{kcal mol}^{-1}$) and that of growth ($105\ \text{kcal mol}^{-1}$). Although the anatase–rutile transformation in the presence of impurities has not been analysed by using JMA theory in the literature, and thus the values of n and k obtained in the present work cannot be compared with previous studies, the small errors in n and k parameters given in Table IV indicate that the transformation is statistically well described by Equation 8. Moreover, the physical meanings of

n and k values support the following conclusion: the anatase–rutile transformation in the presence of Fe_2O_3 is diffusion-controlled, with a decreasing nucleation rate, and with an average activation energy of 110 kcal mol^{-1} (460 kJ mol^{-1}).

4.3. Role of Fe_2O_3 in the phase transition

The foregoing rate laws used to test the experimental data plotted in Fig. 2 describe the transformation reasonably well. However, they do not enable one to understand the role of Fe^{3+} in the transformation on an atomic scale. An analysis of the crystalline structure of anatase and rutile indicates that the transformation involves a collapse of the open anatase structure to a closed rutile structure, with a volume change of about 8%. This process takes place by the rupture of two of the six Ti–O bonds of the titanium coordination octahedra in anatase to form new bonds in rutile, as indicated earlier by Shannon [14]. Hence, the formation of oxygen vacancies should favour the rutile nucleation, as proposed by various authors [6, 12, 16]. Based upon that hypothesis, the enhancement effect of Fe_2O_3 on the phase transition could be understood assuming that Fe^{3+} diffuses in the TiO_2 lattice to form oxygen vacancies, which favour the rutile nucleation. The Fe^{3+} diffusion probably begins in the contact points between Fe_2O_3 and TiO_2 particles on heating anatase in the presence of Fe_2O_3. Literature data support this mechanism because Fe^{3+} is soluble both in anatase and in rutile [26, 27]. The solubility limit of Fe^{3+} in rutile varies between 0.5 and 0.9 at % [24, 25], while in anatase it becomes greater than 1 at % [26, 27]. Moreover, the Fe^{3+} solubility is favoured by the fact that the ionic radii of Fe^{3+} (0.0645 nm, [28]) and Ti^{4+} (0.0605 nm, [28]) are very close. Accordingly, it is reasonable to assume that Fe^{3+} substitutionally replaces Ti^{4+}. Indeed, this substitution has been confirmed by Carter and Okaya [29] and Amorelli *et al.* [30] using electron paramagnetic resonance and electron spin resonance techniques, respectively.

The oxygen vacancies due to Fe^{3+} dissolution in the anatase lattice are probably initially formed at the TiO_2 surface as described by the following reaction

$$Fe_2O_3 = 2Fe'_{Ti} + V_O^{\cdot\cdot} + 3O_O^x \qquad (11)$$

where Fe'_{Ti}, $V_O^{\cdot\cdot}$ and O_O^x denote a charged iron on a titanium site, a doubly charged oxygen vacancy and a neutral anion on an anion site, respectively, in accordance with Kröger and Vink notation [31]. Then, as it occurs in reduced TiO_2, the surface vacancies may rapidly migrate in the TiO_2 bulk [32]. Thus, the vacancies mobility should favour the rutile nucleation in both the surface and the bulk of anatase particles. In addition, the Fe^{3+} diffusion in the TiO_2 bulk, which enhances as the temperature rises [30], should also increase the bulk concentration of oxygen vacancies to keep the charge neutrality. Moreover, an increase in the concentration level of dissolved iron content will favour a greater diffusivity because mass transport in TiO_2 is controlled by oxygen diffusion [33]. According to that, a more rapid growth of rutile phase will be expected from greater Fe^{3+} dissolution and diffusion, which is in agreement with the general theory of the vacancy diffusion mechanism [33] and with measurements performed on chromium-doped TiO_2 [34].

Consequently, when the temperature rises, Fe^{3+} dissolution [35], the concentration of oxygen vacancies and diffusivity in TiO_2 increase. Thus, the nucleation and growth of rutile is favoured by increasing temperature, as shown in Fig. 2. Hence, an analysis of the E_a values determined in this paper can be useful in understanding the relative importance of the three phenomena mentioned. The E_a values of 101–126 kcal mol^{-1} (423–527 kJ mol^{-1}) (models f_1 to f_4) or 135 kcal mol^{-1} (565 kJ mol^{-1}) (Equations 3 and 10 at $\alpha = 0.3$) are greater than the activation energy of Fe^{3+} diffusion in TiO_2 ($E_a = 54$ kcal mol^{-1}) [36, 37] and greater than that of oxygen self-diffusion in TiO_2 ($E_a = 56$ kcal mol^{-1}) [37]. Therefore, these two diffusion phenomena are not relevant in controlling the anatase–rutile transition rate. On the other hand, Marucco *et al.* [38] have reported that the formation of oxygen vacancies in TiO_2 takes place with $E_a = 105$ kcal mol^{-1} (439 kJ mol^{-1}), which is very close to the values of E_a obtained in this paper. Consequently, the E_a values determined in this paper are consistent with a process controlled by the formation of oxygen vacancies rather than a process controlled by diffusion of Fe^{3+} or oxygen self-diffusion.

The importance of oxygen vacancies on the transition rate of TiO_2 in the presence of Fe_2O_3 seems to be also confirmed by a more rapid transformation in argon than in air. In effect, Table I indicates that the transformation was more rapid in argon than in air. Assuming an oxygen partial pressure in argon of 10^{-6} MPa, a deviation from non-stoichiometry $x = 0.0001$ in TiO_{2-x} can be expected [38], oxygen vacancies being the dominant atomic defect [38, 39]. Hence, an argon atmosphere increases oxygen vacancies concentration and thus it favours the anatase transformation. In addition, the iron diffusivity in TiO_{2-x} is significantly increased. In fact, the Fe^{3+} diffusion in TiO_{2-x} at $P_{O_2} \cong 10^{-6}$ MPa is two orders of magnitude more rapid than in TiO_2 in air [39]. Consequently, at 870 °C the Fe^{3+} diffuses in the TiO_{2-x} lattice more rapidly than in stoichiometric TiO_2, which is in agreement with the fact that the atomic-defect structure of TiO_2 significantly influences the mass-transport of impurities [39]. Then, the enhancement effect of Fe^{3+} on the transition in argon may also be attributed to a greater mobility of Fe^{3+} in TiO_{2-x} [33, 39].

4.4. Formation of pseudobrookite: an additional process

The assumption of a model of vacancy formation provides the understanding of the accelerating effect of the Fe^{3+} on the phase transition both in air and in argon. It is further consistent with a great number of publications which have proposed that the formation of oxygen vacancies in pure TiO_2 is the rate-controlling step of the transformation [5, 12, 13, 16].

However, two of these authors [5, 13] have proposed that impurities might form a new dopant-TiO_2 phase, which would act as a nucleating agent for rutile formation. This possibility must be analysed in this paper because an iron titanate known as pseudobrookite, Fe_2TiO_5, was detected on heating the Fe_2O_3–TiO_2 mixtures (Figs 1 and 2). However, from SEM (Fig. 4) and EDXS it was demonstrated that Fe_2TiO_5 layers were formed on Fe_2O_3 particles (Fig. 4). Hence, Ti^{4+} diffuses superficially on to Fe_2O_3 to form Fe_2TiO_5 on the Fe_2O_3 particles. Therefore, the massive Fe_2TiO_5 formation takes place on Fe_2O_3, and thus its formation is independent of the anatase–rutile transformation [40].

5. Conclusion

The anatase–rutile transition in the presence of Fe_2O_3 both in air and argon was more rapid than in pure TiO_2. The accelerating effect of Fe^{3+} in both atmospheres was attributed to the formation of oxygen vacancies produced by Fe^{3+} diffusion in the TiO_2 lattice. In argon, the enhancement effect of Fe^{3+} on the transition was more important because Fe^{3+} diffusion in non-stoichiometric TiO_{2-x} is about two orders of magnitude greater than in stoichiometric TiO_2. The formation of pseudobrookite was independent of the phase transition because it took place on Fe_2O_3 particles.

References

1. J. W. CHRISTIAN, "Theory of transformation in metals and alloys" (Pergamon Press, Oxford, 1965).
2. C. N. R. RAO and K. J. RAO, "Phase transitions in solids" (MacGraw-Hill, New York, 1978).
3. Z. CHVOJ, J. SESTÁK and A. TRISKA, "Kinetic phase diagrams non equilibrium phase transitions" (Elsevier, Amsterdam, 1991).
4. C. N. RAO, S. R. YOGANARASIMHAN and P. A. FAETH, *Trans. Farad. Soc.* **57** (1961) 504.
5. R. D. SHANNON and J. A. PASK, *J. Am. Ceram. Soc.* **48** (1965) 391.
6. K. J. D. MACKENZIE, *Trans. J. Br. Ceram. Soc.* **74** (2) (1975) 29.
7. C. N. R. RAO, A. TURNER and J. M. HONING, *J. Phys. Chem. Solids* **11** (1–2) (1959) 473.
8. S. R. YOGANARASIMHAN and C. N. R. RAO, *Trans. Farad. Soc.* **58** (1962) 1579.
9. Y. IIDA and S. OZAKI, *J. Am. Ceram. Soc.* **44** (1961) 120.
10. O. W. FLÖRKE, *Mitt. Ver. Deut. Emailfachleute* **6** (6) (1958) 49.
11. A. SUZUKI and R. TUKUDA, *Bull. Chem. Soc. Jpn* **42** (1969) 1853.
12. E. F. HEALD and C. W. WEISS, *Am. Mineral.* **57** (1972) 10.
13. K. J. D. MACKENZIE, *Trans. J. Br. Ceram. Soc.* **74** (3) (1975) 77.
14. R. D. SHANNON, *J. Appl. Phys.* **35** (1964) 3414.
15. K. J. D. MACKENZIE, *Trans. J. Br. Ceram. Soc.* **74** (4) (1975) 121.
16. J. ANDRADE GAMBOA and D. M. PASQUEVICH, *J. Am. Ceram. Soc.* **75** (1992) 2934.
17. A. W. CZANDERNA, C. N. RAMACHANDRA RAO and J. M. HONING, *Trans. Farad. Soc.* **54** (1958) 1069.
18. F. P. CORNAZ, J. H. C. VAN HOOFF, F. J. PLUIJIM and C. G. A. SCHUIT, *Discuss. Farad. Soc.* **41** (1966) 290.
19. R. A. SPURR and H. MYERS, *Anal. Chem.* **29** (1957) 760.
20. F. NELLI and D. M. PASQUEVICH, unpublished results.
21. C. N. R. RAO, *Can. J. Chem.* **39** (1961) 498.
22. W. A. JOHNSON and R. F. MEHL, *Trans. AIME* **135** (1939) 416.
23. M. AVRAMI, *J. Chem. Phys.* **7** (1939) 1103.
24. *Idem, ibid.* **8** (1940) 212.
25. *Idem, ibid.* **9** (1941) 177.
26. D. CORDISCHI, N. BURRIESCI, F. D. D'ALBA, M. PETRERA, G. POLIZZOTTI and M. SCHIAVELLO, *J. Solid State Chem.* **56** (1985) 182.
27. R. I. BICKLEY, J. S. LEES, R. J. D. TILLEY, L. PALMISANO and M. SCHIAVELLO, *J. Chem. Soc. Farad. Trans.* **88** (1992) 377.
28. R. D. SHANNON, *Acta Crystallogr.* **A32** (1976) 751.
29. D. L. CARTER and A. OKAYA, *Phys. Rev.* **118** (1960) 1485.
30. A. AMORELLI, J. C. EVANS and C. C. ROWLANDS, *J. Chem. Soc. Farad. Trans. 1* **83** (1987) 3541.
31. E. A. KRÖGER, "The chemistry of imperfect crystals" (Wiley, New York, 1964).
32. P. C. RICHARDSON, R. RUDHAM, A. TULLETT and K. P. WAGSTAFF, *J. Chem. Soc. Farad. Trans. 1* **68** (1972) 2203.
33. P. KOFSTAD, "Nonstoichiometry, diffusion and electrical conductivity in binary metal oxides" (Wiley Interscience, New York, 1972).
34. M. ARITA, M. HOSOYA, M. KOBAYASHI and M. SOMENO, *J. Am. Ceram. Soc.* **62** (1979) 443.
35. E. M. LEVIN, C. R. ROBBINS and H. F. MCMURDIE, "Phase diagrams for ceramists", 3rd Edn (The American Ceramic Society, Columbus, OH, 1964) p. 62.
36. R. S. DE BIASI and M. L. N. GRILLO, *J. Phys. Chem. Solids* **57** (1995) 137.
37. S. MROWEC, "Defects and diffusion in solids: an introduction" (Elsevier Scientific, Amsterdam, 1980).
38. J. F. MARUCCO, J. GAUTRON and P. LEMASSON, *J. Phys. Chem. Solids* **42** (1981) 363.
39. J. SASAKI, N. L. PETERSON and K. HOSHINO, *ibid.* **46** (1985) 1267.
40. F.C. GENNARI, J. J. ANDRADE GAMBOA and D. M. PASQUEVICH, *J. Mater. Sci.* **33** (1998) p. 1563.

Received 18 November 1996
and accepted 27 November 1997